

DETECTION AND ANALYSIS OF SURFACE URBAN COOL ISLAND USING THERMAL INFRARED IMAGERY OF SALATIGA CITY, INDONESIA

Bayu Elwantyo Bagus Dewantoro^{1*}, Panji Mahyatar¹, Wafiq Nur Hayani¹

¹Department of Geographic Information Science, Faculty of Geography, Universitas Gadjah Mada, Yogyakarta, 55281, Indonesia

*e-mail: bayuelwantyo@mail.ugm.ac.id

Received: 13 August 2020; Revised: 10 November 2020; Accepted: 17 December 2020

Abstract. The detection and monitoring of the dynamics of urban micro-climates needs to be performed effectively, efficiently, consistently and sustainably in an effort to improve urban resilience to such phenomena. Thermal remote sensing possesses surface thermal energy detection capabilities which can be converted into surface temperatures and utilised to analyse the urban micro-climate phenomenon over large areas, short periods of time, and at low cost. This paper studies the surface urban cool island (SUCI) effect, the reverse phenomenon of the surface urban heat island (SUHI) effect, in an effort to provide cities with resistance to the urban microclimate phenomenon. The study also aims to detect urban micro-climate phenomena, and to calculate the intensity and spatial distribution of SUCI. The methods used include quantitative-descriptive analysis of remote sensing data, including LST extraction, spectral transformation, multispectral classification for land cover mapping, and statistical analysis. The results show that the urban micro-climate phenomenon in the form of SUHI in the middle of the city of Salatiga is due to the high level of building density in the area experiencing the effect, which mostly has a normal surface temperature based on the calculation of the threshold, while the relative SUCI occurs at the edge of the city. SUCI intensity in Salatiga ranges between -6.71°C and 0°C and is associated with vegetation.

Keywords: *Thermal Remote Sensing, Land Surface Temperature, Urban Microclimate, Surface Urban Cool Island*

1 INTRODUCTION

The urbanization phenomenon has a significant impact on increases in surface temperature, meaning cities are vulnerable to changes in microclimate characteristics, which can lead to environmental problems (Wang et al., 2016; Huang & Wang, 2019). A microclimate is a climatic condition in the local atmospheric zone which exhibits differences to the surrounding environment (Chen et al., 1999; Ismangil et al., 2016). The change in microclimate is one of the types of pressure faced by cities, as it is related to the urban heat island (UHI), which is a phenomenon in which the temperature of

the urban area is higher than the surrounding rural areas (Xian & Crane, 2006; Mostofi & Hasanlou, 2017). UHI also has other negative impacts, such as changing air quality, effect on human health, and energy exchange (Lai & Cheng, 2009; Road et al., 2010; Stone et al., 2010; Tan et al., 2010; Skelhorn et al., 2016; Ng & Ren, 2017; Fawzi, 2017). It eventually also disrupts the comfort of life in urban areas.

In recent years, the study of micro-climate change has been much more focused on the UHI phenomenon. However, few studies have considered the urban cool island (UCI) effect, which is the opposite of UHI and is a phenomenon

whereby the air temperature in the countryside is higher than in the urban area (Yang et al., 2016). Several previous studies have suggested that UCI is effective for the microclimate mitigation, reducing rising air temperatures, and improving the comfort of urban areas (Cao et al., 2010; Kong, et al., 2014). Therefore, UCI can also be used to plan the provision of green open spaces and to improve the effectiveness of monitoring the dynamics of climate changes in an effort to improve cities' resilience to microclimate change.

Few studies on UCI have been conducted in Indonesia, especially in relation to the city of Salatiga. This was one of the cities in Central Java province which in 2020 was a pilot nationally and internationally for the integration of the development of green open spaces. The city managed to exceed the national target for the provision of green open space by 24%, of which 16.11% was combined green open space, with the remainder being sustainable development agricultural land. This condition makes Salatiga an interesting location for research on UCI, considering RTH has an influence on the surface temperature of cities.

Study of UCI is differentiated into two types: UCI surface and UCI water. The surface intensity of UCI, commonly abbreviated as SUCI, can be gauged directly from the land surface temperature (LST) value of data extraction recorded by infrared thermal sensor satellite remote sensing. LST is an energy beam of ground level objects successfully recorded by sensors (Li et al., 2013; Alhawiti, 2016). On the other hand, UCI water requires different data to LST, namely the air temperature, usually obtained from measurements in the field or from station climatology. Remote sensing applications for SUCI/UCI research are almost the same as those for SUHI/UHI research, mostly

employing cover/land use as one of its variants. For example, Reisi et al. (2019) examined the effect of LULC (landuse/landcover) changes on LST in Isfahan City, Iran, from 1985 to 2017, using Landsat 5 and 7 ETM imagery. However, the results in their study did not further assess SUCI/UCI intensity. The study of such intensity has been more detailed in previous years. For instance, Li and Dai (2011) measured UCI intensity based on the boundary line changes of several cities in Hunan, China in 1989, 2001 and 2006. Their results showed that the difference in the city boundary line affected UCI intensity up to a maximum of > 2 °C. In addition, the negative correlation between NDVI and UCI intensity was also established by Li and Dai (2011), even though the coefficient of the correlation decreased from 0.845 to 0.606. The results of their study is shown only in table form and are not visualized spatially in the form of maps, so the spatial distribution is unknown.

The association between UCI and green open space was examined by Chen et al. (2014) in Beijing, China, whose research results showed the influence of urban RTH spatial patterns on UCI, and that these were stronger during winter. The pattern size and combination of RTH vegetation also influenced UCI. More complex research was conducted by Rasul et al. (2015), who examined the influence of LST on SUCI in the dry season using several spectral transformations, which included wetness, brightness, the greenness index, NDBI and NDVI. Their results show that the brightness index was a very influential factor in the LST, while the wetness index was the second factor. In addition, the LST with NDBI had a strong positive correlation, whereas NDVI-based LST had a negative correlation.

The purpose of this SUCI research in the city of Salatiga using the remote sensing approach is (1) to, establish the

spatial distribution of SUCI intensity; and (2) to calculate this intensity.

2 MATERIALS AND METHODOLOGY

2.1 Location and Data

The research site was located in Salatiga City, Central Java province, Indonesia, with coordinates of between $07^{\circ}17' - 07^{\circ}17'23''$ S and $110^{\circ}27'57'' - 110^{\circ}32'05''$ E. The city is completely bordered by Semarang Regency, Central Java province. It has a total area of 56.78 km², of which 24% is green open space (see Figure 2-1).

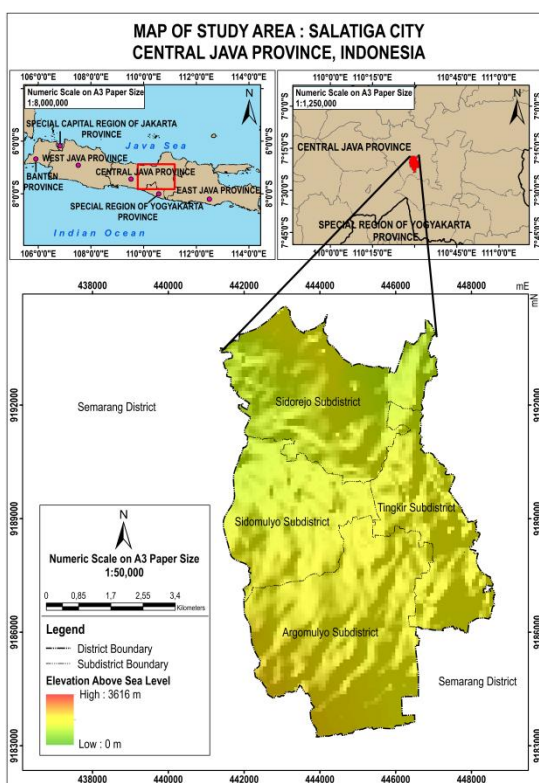


Figure 2-1: Location of Study Area

The imagery used in the research was obtained from Landsat 8 OLI/TIRS with a resolution of 30 m (*pixel resampling from Earth Engine Dataset*) with a recording date of 16 November 2019, and Sentinel 2A MSI with a resolution of 10 m, with a recording date of 19 November 2019. The selection of the dates was based on the availability of data with minimum cloud cover to produce objective analysis. The Landsat 8 OLI Thermal Infrared Sensor (TIRS) was

employed for the Land Surface Temperature (LST) estimation used for Surface Urban Cool Island (SUCI) analysis, and data with 1-7 multispectral bands used for the creation of the vegetation index transformation. Sentinel 2A MSI images were used for the classification of land cover in the study area.

Landsat 8 and Sentinel 2A were not used for comparison analysis. Landsat 8 focused on thermal imagery analysis covering LST to SUCI, while land cover from Sentinel 2A was only used to observe SUCI spatial distribution of certain land cover classes. Sentinel 2A was selected for land cover classification with the aim of improving its accuracy.

2.2 Radiometric and Geometric Correction

Landsat 8 OLI/TIRS Imagery and Sentinel 2A MSI were atmospherically corrected to surface reflectance (*bottom-of-atmosphere*). The atmospheric corrected imagery from Landsat 8 OLI/TIRS was used for spectral transformation purposes, while Sentinel 2A MSI was used for the multispectral classification of land cover. The image products used were also geometrically corrected, so it was only necessary to make an overview check to ensure the geometric position of both the images was precise and relevant to be processed based on the 1:25,000 scale Rupabumi Indonesia map of Salatiga City. The imagery used is available on the Google Earth Engine (GEE) platform

2.3 Land Surface Temperature Extraction

Land Surface Temperature (LST) extraction was performed on the Google Earth Engine using the Single Channel Algorithm (SCA) method, based on its ease of accessibility, efficiency and effectiveness in data acquisition.

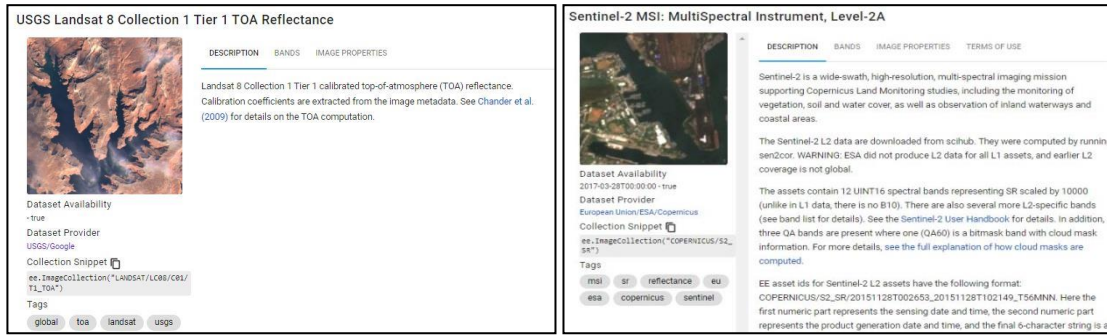


Figure 2-2: Image Metadata Collection in Google Earth Engine
 Source: <https://developers.google.com/earth-engine/datasets>

The extraction was performed on the Landsat 8 TIRS imagery using thermal channel Band 10. According to Loyd (2017), cited in Fawzi (2017), band 10 has a thermal accuracy of $\sim \pm 1$ Kelvin for simple LST estimation at the urban scale or greater. The thermal imagery acquired from GEE was already a brightness temperature (T_{rad}) as a result of the calibration of at-sensor spectral radiance ($L\lambda$).

The brightness temperature of the extraction used Kelvin units to facilitate the analysis; the conversion of the units to Celsius ($^{\circ}C$) was made with the following formula:

$$T_{celsius} = T - 273.15 \quad (2-1)$$

where:

- $T_{celsius}$ = temperature in Celsius ($^{\circ}C$)
- T = temperature in Kelvin (K)

The extraction of surface temperature needs to be made through the emissivity correction process to obtain accurate values (Fawzi, 2017). One method for the correction of emissivity is use of the vegetation index NDVI (Salih et al., 2018; Bahi et al., 2016; Fawzi, 2017). The formula used to compose the NDVI in Landsat 8 OLI is as follows:

$$NDVI = \frac{(B5 - B4)}{(B5 + B4)} \quad (2-2)$$

where:

- $B5$ = NIR Band
- $B4$ = Red Band

An emissivity correction method using NDVI requires the values of vegetation and soil emissivity. Referring to Fawzi (2017), the vegetation values in the measurement results were in the range of $\epsilon_v = 0.980 - 0.990$, while for soil emissivity in the range of $\epsilon_s = 0.950 - 0.970$. The calculation of the surface emissivity value to be used in the LST estimation refers to the following formulas (Salih et al., 2018; Li & Norford 2016; Sobrino et al., 2008; Valor, 1996):

$$\epsilon = \epsilon_v P_v + \epsilon_s (1 - P_v) + d\epsilon \quad (2-3)$$

where:

- ϵ = land surface emissivity
- ϵ_v = emissivity of vegetation
- ϵ_s = emissivity of soil
- P_v = proportion of vegetation
- $d\epsilon$ = surface roughness

$$P_v = \left(\frac{NDVI - NDVI_s}{NDVI_v - NDVI_s} \right)^2 \quad (2-4)$$

where:

- P_v = proportion of vegetation
- $NDVI_s$ = spectral value of soil in NDVI
- $NDVI_v$ = spectral value of vegetation in NDVI

The last phase of the LST extraction process involves inclusion of all the necessary variables in the following equation (Salih et al., 2018):

$$LST = \frac{T_{rad}}{\left(1 + \left(\frac{T_{rad}}{p} \right) \ln \epsilon \right)} \quad (2-5)$$

where:

- LST = land surface temperature (°C)
- T_{rad} = brightness temperature (°C)
- P = constant of 1.488 x 10⁻²
- ε = surface emissivity

2.4 Detection of Area Indicated by Surface Urban Heat and Cool Island (SUHI/SUCI)

Initial detection and identification of surface urban heat and cool island (SUHI/SUCI) can be made visually by observing the LST distribution patterns, but for the purpose of mitigation and planning of areas related to urban microclimate phenomena it is necessary that heat and cool islands are accommodated in quantitative form. Lima and Lopes (2017) used the following formula for early detection of areas indicated as SUHI/SUCI:

$$\Delta T_{\mu-r} = T_{\mu} - T_r \quad (2-6)$$

where:

- ΔT_{μ-r} = LST difference in the area indicated by SUHI (°C)
- T_μ = LST difference in urban area (°C)
- T_r = LST difference in nonurban area (°C)

$$\Delta T_{r-\mu} = T_r - T_{\mu} \quad (2-7)$$

where:

- ΔT_{r-μ} = LST difference in the area indicated by SUCI (°C)
- T_μ = LST difference in urban area (°C)
- T_r = LST difference in non-urban area (°C)

Equation (6) was used to identify the surface temperature of the area indicated by the SUHI phenomenon, while equation (7) was used to identify the surface temperature in the area indicated by SUCI. These equations are simple one to ascertain the surface temperature difference in the early detection of the

SUHI/SUCI phenomena ; it needs a formula to find the SUHI/SUCI intensity to obtain the surface temperature threshold as the basis for the analysis.

Research conducted by Ma et al. (2010) used a more specific formula related to determining the surface temperature threshold in the SUHI/SUCI phenomena, as follows:

$$T_{suhi} > \mu_{ori} + 0,5\alpha_{ori} \quad (2-8)$$

where:

- T_{suhi} = LST in the area indicated by SUHI (°C)
- μ_{ori} = average of LST in the original thermal image (°C)
- α_{ori} = standard deviation in the original thermal image

Equation (8) was used to obtain a surface temperature threshold on an indicated area of SUHI.

$$0 < T_{norm} \leq \mu_{ori} + 0,5\alpha_{ori} \quad (2-9)$$

where:

- T_{norm} = LST in normal condition (°C)
- μ_{ori} = average of LST in the original thermal image (°C)
- α_{ori} = standard deviation in the original thermal image

Equation (9) was used to obtain the surface temperature threshold in regions not indicated as SUHI. The area that is included in this surface temperature range has not been identified as SUCI because it still has the potential to become an area with normal surface temperature, or a SUCI indication area.

The determination of the SUCI surface temperature threshold requires statistical surface temperatures in areas with normal conditions to determine the distribution of surface temperature values and central tendencies. Equations that can be reduced to acquire threshold values in the SUCI-indicated areas are as follows:

$$T_{Suci} < \mu_{norm} + 0,5\alpha_{norm} \quad (2-10)$$

where:

T_{suci} = LST in the area indicated by SUCI (°C)

μ_{norm} = average of LST in the original thermal image with normal condition (°C)

α_{norm} = standard deviation in thermal image with normal condition

Table 2-1: Average, StDev and Threshold Values of SUHI, Normal and SUCI

	Average	StDev
Toriginal (°C)	30.09	4.68
Tnormal (°C)	27.21	3.02
SUHI Threshold (°C)	T > 32.43	
Normal Threshold (°C)	28.72 ≤ T ≤ 32.43	
SUCI Threshold (°C)	T < 28.72	

2.5 Measuring Surface Urban Cool Island (SUCI) Intensity

The value of the surface temperature threshold was obtained as the basis for the spatial measurement of SUCI intensity. This intensity was obtained by using a modified equation from Fawzi's (2017) study, as follows:

$$SUCI_{in} = T_{suci} - (\mu_{norm} + 0,5\alpha_{norm}) \quad (2-11)$$

where:

$SUCI_{in}$ = SUCI Intensity (°C)

T_{suci} = LST in the area indicated by SUCI (°C)

μ_{norm} = average of LST in the original thermal image in normal conditions (°C)

α_{norm} = standard deviation in the original thermal image in normal conditions

2.6 Land Cover Classification and Accuracy Assessment

Land cover classification was performed using the supervised

classification method with the maximum likelihood algorithm. The classification was divided into three class: bare land, built up areas and vegetation. This algorithm was selected based on its good performance in land cover classification based on probability calculation or the maximum probability of each sample group (Danoedoro, 2012).

The accuracy assessment of the land cover map was made using a confusion matrix and kappa coefficient. Sampling for the assessment was made using the cross-validation method, which was performed by different people so the results were more objective. This was also because of the small number of land cover classes with many different characteristics. The sampling method used in the accuracy assessment was stratified random sampling, with a total sample of 22,686 pixels divided into 15,886 model samples and 6,800 accuracy samples.

3 RESULTS AND DISCUSSION

3.1 Spatial Distribution of LST and Land Cover in Salatiga City

The results of the processing of the Landsat 8 TIRS thermal imagery indicates that the surface temperature is high enough in the central area of Salatiga that for it to be visually identified against the LST distribution pattern. The distribution of LST is quite high between 30°C - 37°C, concentrated in the middle of the city, which is influenced by the densely built-up area. This increases the emissivity of the surface, which is recorded by the thermal infrared sensor as a higher surface temperature than that in the surrounding area. The built-up area spatial pattern also affects the surface temperature distribution, as shown in the image in this figure.

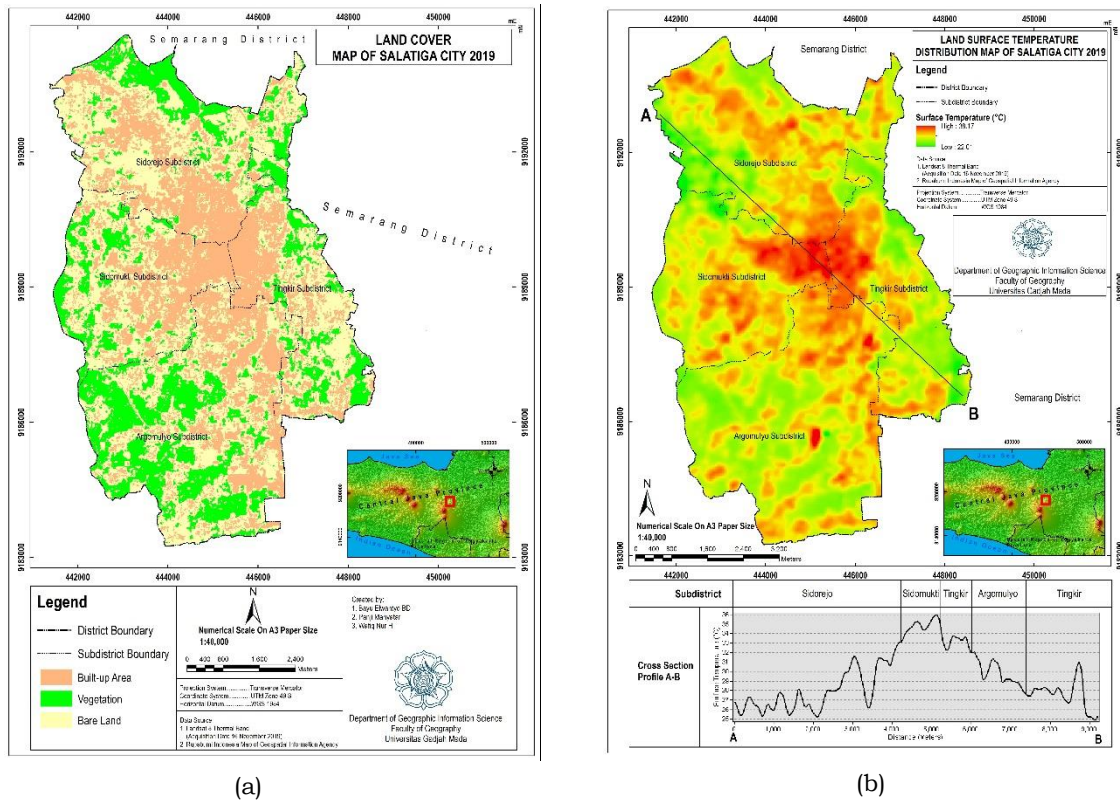


Figure 3-1: Land cover (a) and LST (b) on map of Salatiga City

The patterns of the LST values are quite high in the central part of the city, where the land cover is dominated by built-up areas, while the edge of the city tends to have a lower surface temperature, with a dominance of vegetation. This shows that there is a difference in the thermal energy emitted from the built-up area and the area with vegetation, as seen in Figure 3-1.

3.2 Detection of SUHI Area, Normal Condition and SUCI

The detection process of the area indicated by SUHI, the normal condition and SUCI is based on the equations used and the threshold value of the surface temperature. The results of the processing indicate that the potential occurrence of SUHI is in areas with a surface temperature of $>32.43^{\circ}\text{C}$, which are distributed in the center of the city, while the surface temperatures in normal conditions are in the range of 28.72°C - 32.43°C , and are spread around the region with potential SUHI.

Indications of SUCI were detected on the edge of the city, with a surface temperature of $<28.72^{\circ}\text{C}$. These indications have a pattern that tends to group on the city edge, with land cover in the form of vegetation and some bare land. SUCI intensity measurements were taken to obtain specific information related to SUCI.

Based on the measurement results, SUCI intensity was divided into five classes : very high (-6.71°C - -5.37°C); high (-5.36°C - -4.03°C); medium (-4.02°C - -2.68°C); low (-2.67°C - -1.34°C); and very low (-1.33°C - 0°C). The intensity shows the SUCI effect that occurs in related areas. It is very high, signifying that the area has a greater SUCI effect than the surrounding area, with a difference in the value of the surface temperature of between -6.71°C to -5.37°C . The dominance of land cover in areas of high intensity value in the form of vegetation with varying levels of greenish.

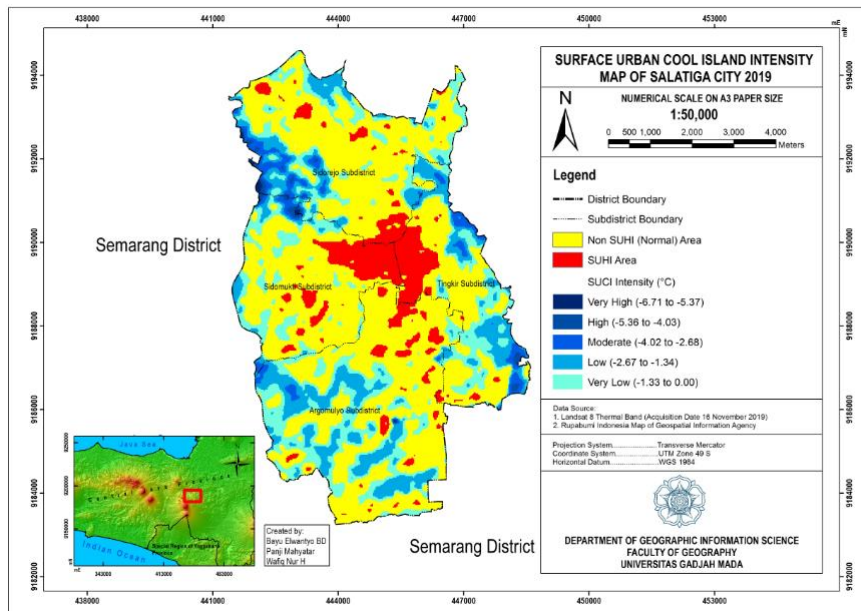


Figure 3-2: SUCI Intensity Map of Salatiga City

Table 3-1: Accuracy Assessment of Land Cover Map
Ground Truth (Pixels)

		Vegetation	Built up Area	Bare land	Total row	User Accuracy (%)
Tentative Map	Vegetation	1932	100	256	2288	84.44
	Built up Area	224	1957	34	2215	88.35
	Bare land	140	117	2040	2297	88.81
	Total column	2296	2174	2330	6800	
	Producer Accuracy (%)	84.15	90.02	87.55		
	Overall Accuracy (%)	87.19				

3.3 Accuracy Assessment of the Land Cover Map

The land cover map accuracy test was conducted using a confusion matrix and kappa coefficient. The accuracy assessment results show good accuracy with the kappa coefficient, in the very good agreement category. The accuracy assessment results can be seen in Table 3-1.

3.4 Accuracy Assessment of Land Surface Temperature (LST)

Some researchers suggest that the accuracy test and validation of that surface temperature should be conducted a maximum of 3-4 hours after recording (for addition, Sabins, 2007, cited in Fawzi, 2017), even though the surface temperature is very dynamic, even in seconds. Ideally, an accuracy test should

be made simultaneously when the satellite is recording the area, but this is very difficult to achieve.

There is also the option to make comparisons of two thermal infrared sensors that record the same area, but due to data source limitations, this is also difficult to do. Studies on surface temperature accuracy tests need to be reviewed in relation to the extraction process. Accuracy testing of remote sensing imagery is made only on the results of both visual and digital interpretation; for example, on the interpretation of land cover/land use. Land cover/land use is a hybrid variable that needs to be tested, while the biophysical variables that make up the hybrid variable are sets of pixel values that do not need to be tested (Danoedoro, 2012).

Table 3-2: Calibration constant of Landsat 8 TIRS Band 10

Temperature (K)	TIRS Band10 Change in Response (K)	
	Feb 11, 2013 – Mar 1, 2015	Mar 2, 2015 - Present
240 (extrapolated)	-0.11	2.73
273	0.08	1.05
285	0.14	0.60
300	0.20	0.12
320 (extrapolated)	0.27	-0.42

Source: <https://www.usgs.gov/core-science-systems/nli/landsat/landsat-8-oli-and-tirs-calibration-notice>

Related to this issue, land surface temperature is a biophysical variable derived from inversions in physics equations, so there is no need to test its accuracy as long as the equations are used correctly according to established procedure. Another example of a biophysical variable is the pixel value in the images of the NDVI vegetation index transformation results. This value does not need to be tested because it is a biophysical variable derived from an equation, and a variable used as interpretation material to compose the hybrid variable. When accuracy tests are made on land surface temperature (LST), these are performed to test the thermal infrared sensor used in terms of its accuracy in relation to the actual temperature in the field, and not to test the land surface temperature (LST) itself (Danoedoro, 2012).

Based on these issues, the United States Geological Survey has routinely calibrated the TIRS sensors attached to Landsat 8, with the results shown in Table 3-2.

Based on Table 3-2, the accuracy of the TIRS sensor in Landsat 8 Band 10 is an average of 0.466 K. This shows that the analysis using land surface temperature data derived using Landsat 8 TIRS Band 10 has an estimated value of 0.466 K warmer than the original condition.

4 CONCLUSION

The phenomenon of SUHI in Salatiga was detected in the centre of the city, which was surrounded by areas with normal surface temperature based on the threshold value, while SUCI was distributed on the edge of the city, with an intensity -6.71°C to 0°C , and was associated with vegetation.

ACKNOWLEDGEMENTS

The authors would like to thank the United States Geological Survey for providing free-access data. We also would like to express our gratitude to the reviewer and editorial team.

AUTHOR CONTRIBUTIONS

Detection and Analysis of Surface Urban Cool Island Using Thermal Infrared Imagery of Salatiga City, Indonesia. Lead Author: Bayu Elwantyo Bagus Dewantoro, Co-Author: Panji Mahyatar and Wafiq Nur Hayani. Author contributions are as follows:

1. Bayu Elwantyo Bagus Dewantoro: Thermal image processing, map layouting, and results analysis
2. Panji Mahyatar: Provision and processing of optical imagery
3. Wafiq Nur Hayani: Provision of introductions and prepare draft manuscripts

REFERENCES

- Adachi, S.A., Kimura, F., Kusaka, H., Inoue, T., & Ueda, H. (2012). Comparison of the impact of global climate changes and urbanization on summertime future climate in the Tokyo metropolitan area. *American Meteorological Society*, 7, 1441-1454, <https://doi.org/10.1175/JAMC-D-11-0137.1>.
- Alhawiti, R. H., & Mitsova, D. (2016). Using Landsat-8 Data to Explore The Correlation Between Urban Heat Island and Urban Land Uses. *IJRET: International Journal of Research in Engineering and Technology*, 5(3), 457-466.
- Bahi, H., Hassan, R., Ahmed, B., Ute, F., & Dieter, S. (2016). Effects of Urbanization and Seasonal Cycle on the Surface Urban Heat Island Patterns in the Coastal Growing Cities: A Case Study of Casablanca, Morocco. *Remote Sensing*, 8(829), 1-26. doi:10.3390/rs8100829.
- Cao, X., Onishi, A., Chen, J., & Imura, H. (2010). Quantifying the Cool Island Intensity of Urban Parks Using ASTER and IKONOS Data. *Landscape and Urban Planning*, 96(4), 224-231.
- Chen, A., Yao, X. A., Sun, R., & Chen, L. (2014). Effect of Urban Green Patterns on Surface Urban Cool Islands and Its Seasonal Variations. *Urban Forestry & Urban Greening*, 13(4), 646-654. <https://doi.org/10.1016/j.ufug.2014.07.006>.
- Chen, J., Saunders, S.C., Crow T.R., Naiman, R.J., Brosofske, K.D., Mroz G.D., Brookshire, B.L., & Franklin, J.F. (1999). Microclimate in forest Ecosystem and Landscape Ecology: Variations in local climate can be used to monitor and compare the effects of different management regimes. *BioScience*, 49(4), 288-297.
- Danoedoro, P. (2012). *Pengantar penginderaan jauh digital [Introduction to digital remote sensing]*. Yogyakarta: Andi.
- Fawzi, N. I. (2017). Mengukur urban heat island menggunakan penginderaan jauh, kasus di Kota Yogyakarta [Measuring urban heat island using remote sensing, a case in Yogyakarta City]. *Majalah Ilmiah Globè*, 19(2), 195-206.
- Goggins, W.B., Chan, E.Y.Y., Ng, E., Ren, C., & Chen, L., (2012). Effect modification of the association between short-term meteorological factors and mortality by urban heat islands in Hong Kong. *PLOS ONE*, 7(6), 1 - 6. <https://doi.org/10.1371/journal.pone.0038551>.
- Huang, X., & Wang, Y. (2019). Investigating The Effects of 3D Urban Morphology on The Surface Urban Heat Island Effect in Urban Functional Zones by Using High-Resolution Remote Sensing Data: A Case Study of Wuhan, Central China. *ISPRS Journal of Photogrammetry and Remote Sensing*, 152, 119-131. <https://doi.org/10.1016/j.isprsjprs.2019.04.010>.
- Ismangil, D., Wiegant, D., Hagos, E., Steenbergen, F.V., Kool, M., Sambalino, F., Castelli, G., Bresci, E., & Hagos F. (2016). Managing the Microclimate. Spate Irrigation Network Foundation.
- Kong, F., Yin, H., Wang, C., Cavan, G., & James, P. (2014). A Satellite Image-Based Analysis of Factors Contributing to The Green-Space Cool Island Intensity on A City Scale. *Urban Forestry & Urban Greening*, 13(4), 846-853. <http://dx.doi.org/10.1016/j.ufug.2014.09.009>.
- Lai, L.W., & Cheng, W.L. (2009). Air Quality Influenced by Urban Heat Island Coupled with Synoptic Weather Patterns. *Science of the Total Environment*, 407(8), 2724-2733.
- Li, S., Mo, H., & Dai, Y. (2011). Spatio-Temporal Pattern of Urban Cool Island Intensity and Its Eco-environmental Response in Chang-Zhu-Tan Urban Agglomeration. *Communications in Information Science and Management Engineering*, 1(9), 1-6.
- Li, X.X., & Norford, L.K.. (2016). Evaluation of cool roof and vegetations in mitigating

- urban heat island in a tropical city, Singapore. *Urban Climate*, 16, 59–74.
- Li, Z-L, Tang, B-H, Wu, H., Ren, H., Yan, G., Wan, Z., Trigo, I.F., & Sobrino, J.A. (2013). Satellite-Derived Land Surface Temperature: Current Status and Perspectives. *Remote Sensing of the Environment*, 131, 14-37. <http://dx.doi.org/10.1016/j.rse.2012.12.008>.
- Lima, A. E., & Lopes, A. (2017). The urban heat island effect and the role of vegetation to address the negative impact of local climate changes in a small Brazilian City. *Atmosphere Multidisciplinary Digital Publishing Institute* 8(2), 1-14
- Loyd, C.. (2017). Landsat 8 bands. Landsat Science. Available at: <https://landsat.gsfc.nasa.gov/landsat-8/landsat-8-bands/>. Accessed 19 June 2020.
- Ma, Y., Kuang, Y., & Huang, N. (2010). Coupling urbanization analyses for studying urban thermal environment and its interplay with biophysical parameters based on tm/etm+ imagery. *International Journal of Applied Earth Observation and Geoinformation* 12(2): 110–118.
- Mostofi, N., & Hasanlou, M. (2017). Feature Selection of Various Land Cover Indices for Monitoring Surface Heat Island in Tehran City Using Landsat 8 Imagery. *Journal of Environmental Engineering and Landscape*, 25(3), 1-10. <http://dx.doi.org/10.3846/16486897.2016.1223084>.
- Ng, E., & Ren, C. (2017). China's Adaptation to Climate & Urban Climatic Changes: A Critical Review. *Urban Climate*, 23, 352 – 372. <https://doi.org/10.1016/j.uclim.2017.07.006>.
- Rasul, A., Balzter, H., & Smith, C. (2015). Spatial Variation of The Daytime Surface Urban Cool Island During The Dry Season in Erbil, Iraqi Kurdistan, from Landsat 8. *Urban Climate*, 14(2), 176-186. <http://dx.doi.org/10.1016/j.uclim.2015.09.001>.
- Reisi, M., Nadoushan, M. A., & Aye, L. (2019). Remote Sensing for Urban Heat and Cool Islands Evaluation in Semi-Arid Areas. *Global Journal of Environmental Science and Management*, 5(3), 319-330. doi: 10.22034/gjesm.2019.03.05.
- Kershaw, T., Sanderson, M., Coley, D., Eames, M. (2010). Estimation of The Urban Heat Island for UK Climate Change Projections. *Building Services Engineering Research and Technology*, 31(3), 251–263.
- Sabins, F. F. (2007). *Remote Sensing: Principles and Interpretation 3rd Edition*. Illinois: Waveland Press.
- Salih, M. M., Jasim, O. Z., Hassoon, K. I., & Abdalkadhum, A. J. (2018). Land surface temperature retrieval from Landsat-8 thermal infrared sensor data and validation with infrared thermometer camera. *International Journal of Engineering and Technology*, 7(4.2), 608 – 612, doi: 10.14419/ijet.v7i4.20.27402.
- Skelhorn, C. P., Lindley, S. & Levermore, G. (2016). Urban Greening and the UHI: Seasonal Trade-Offs in Heating and Cooling Energy Consumption in Manchester, UK. *Urban Climate*, 23, available at: <https://doi.org/10.1016/j.uclim.2017.02.010>.
- Stone, B., Hess, J.J., & Frumkin, H. (2010). Urban Form and Extreme Heat Events: Are Sprawling Cities More Vulnerable to Climate Change than Compact Cities? *Environmental Health Perspectives*, 118(10), 1425–1428.
- Sobrino, J. A., Jimenez-Munoz, J. C., Soria, G., Romaguera, M., Guanter, L., Plaza, A., & Martinez, P. (2008). Land surface emissivity retrieval from different VNIR and TIR sensors. *IEEE Transactions on Geoscience and Remote Sensing* 46, 316 – 327.
- Tan, J., Zheng, Y., Tang, X., Guo, C., Li, L., Song, G., Zhen, X., Yuan, D., Kalkstein, A.J., & Li, F. (2010). The Urban Heat Island and

- Its Impact on Heat Waves and Human Health in Shanghai. *International Journal of Biometeorology*, 54(1), 75–84.
- Tran, H., Uchihama, D., Ochi, S., & Yasuoka, Y., (2006), Assessment with satellite data of the urban heat island effects in Asian mega cities. *International Journal of Applied Earth Observation and Geoinformation* 8(1), 34-48. <https://doi.org/10.1016/j.jag.2005.05.003>.
- Valor, E., & Caselles, V. (1996). Mapping land surface emissivity from NDVI: Application to European, African, and South American areas. *Remote Sensing of Environment* 57(3), 167–184.
- Wang, Y., Chen, L., & Kubota, J. (2016). The Relationship Between Urbanization, Energy Use and Carbon Emissions: Evidence from A Panel of Association of Southeast Asian Nations (ASEAN) Countries. *Journal of Cleaner Production*, 112, 1368–1374.
- Xian, G., & Crane, M. (2006). An Analysis of Urban Thermal Characteristics and Associated Land Cover in Tampa Bay and Las Vegas Using Landsat satellite Data. *Remote Sensing of Environment* 104(2), 147–156. <https://doi.org/10.1016/j.rse.2005.09.023>
- Yang, X., Li, Y., Luo, Z., & Chan, P. W. (2016). The Urban Cool Island Phenomenon in A High-Rise High-Density and Its Mechanism. *International Journal of Climatology*, 37(2), 890–904. <https://doi.org/10.1002/joc.4747>.